Advances in Aircraft and Spacecraft Science, *Vol. 10, No. 6 (2023) 521-543*
https://doi.org/10.12989/aas.2023.10.6.521

Reynolds stress correction by data assimilation methods with physical constraints

Thomas Philibert[1,2,3a], Andrea Ferrero*[2], Angelo Iollo[1,3b] and Francesco Larocca[2c]

[1]*Institut National de Recherche en Informatique et en Automatique*, *200 Av. de la Vieille Tour*, *Talence*, *France*
[2]*Department of Mechanical and Aerospace Engineering*, *Politecnico di Torino*,
Corso Duca degli Abruzzi 24, *Torino*, *Italy*
[3]*Institut de Mathématiques de Bordeaux*, *Université Bordeaux*, *Cours de la Libération*, *351*, *Talence*, *France*

(Received December 1, 2023, Revised January 5, 2024, Accepted January 15, 2024)

Abstract. Reynolds-averaged Navier-Stokes (RANS) models are extensively employed in industrial settings for the purpose of simulating intricate fluid flows. However, these models are subject to certain limitations. Notably, disparities persist in the Reynolds stresses when comparing the RANS model with high-fidelity data obtained from Direct Numerical Simulation (DNS) or experimental measurements. In this work we propose an approach to mitigate these discrepancies while retaining the favorable attributes of the Menter Shear Stress Transport (SST) model, such as its significantly lower computational expense compared to DNS simulations. This strategy entails incorporating an explicit algebraic model and employing a neural network to correct the turbulent characteristic time. The imposition of realizability constraints is investigated through the introduction of penalization terms. The assimilated Reynolds stress model demonstrates good predictive performance in both in-sample and out-of-sample flow configurations. This suggests that the model can effectively capture the turbulent characteristics of the flow and produce physically realistic predictions.

Keywords: machine learning; non-linear closure; RANS; realizability conditions; turbulence modeling

1. Introduction

Several problems in the field of aerospace engineering require reliable tools for turbulence modeling to develop more efficient systems. However, a dilemma must be faced: either accurate models such as direct numerical simulations (DNS) or large-eddy simulations (LES) are used, which are very expensive in terms of computational time, or less accurate but faster models such as Reynolds-averaged Navier-Stokes models (RANS) can be adopted. RANS models reach their limits when considering flows characterised by separations or transition. It is therefore necessary to improve these models, and one promising way is to use data-driven approaches with modern assimilation tools.

One of the strengths, but also one of the limiting factors, of RANS models is that they use the

*Corresponding author, Assistant Professor, E-mail: andrea_ferrero@polito.it
[a]Ph.D. Student, E-mail: thomas.philibert@polito.it
[b]Professor, E-mail: angelo.iollo@inria.fr
[c]Associate Professor, E-mail: francesco.larocca@formerfaculty.polito.it

http://www.techno-press.org/?journal=aas&subpage=7 ISSN: 2287-528X (Print), 2287-5271 (Online)

Boussinesq approximation as a closure model. This approximation is convenient because it is easy to compute since it states that the anisotropic part of the Reynolds stress tensor is linearly dependent on the strain rate tensor. However, when looking at high-fidelity data, it can be shown that this approximation is not always verified. A way to improve this approximation was proposed by Pope (1975) and was exploited for the development of a new family of non-linear closure models known as explicit algebraic Reynolds stress models (EARSMs). This approach uses a tensor basis that enforces Galilean invariance. The invariance is an essential property since it ensures that the results of the experiments and observations should be the same regardless of the coordinate system or observer motion. Various machine learning techniques have been used to improve Pope's assumption. In general data-augmented turbulence models involve compensating for model errors by incorporating high-fidelity data to train correction terms as suggested by Xiao and Cinnella (2019). Ling and Templeton (2015) introduced classifiers that can identify regions where turbulence models exhibit low accuracy or violate model assumptions by using direct numerical simulation (DNS) and large eddy simulation (LES) solutions. Wang *et al.* (2017) employed machine learning to directly correct the Reynolds stress tensor based on mean flow features, leading to improved accuracy even on different test cases. Similarly, Sandberg and Michelassi (2019) and Sandberg and Weatheritt (2014) used an evolutionary algorithm to obtain the coefficients within the framework of the EARSM model. In another approach, Wu *et al.* (2017) utilized a random forest model to estimate the confidence of RANS solutions before prediction.

Similarly, Ling *et al.* (2016) proposed a method to correct the Reynolds stress tensor using a neural network structure with embedded invariance properties. This concept was later extended to a more comprehensive, albeit computationally expensive, framework by Wu *et al.* (2018). However, a limitation of the aforementioned methods is that they learn corrections directly from high-fidelity data, which may lead to inconsistencies with RANS model structures. To address this issue and ensure consistency, data-assimilation (DA) techniques based on inverse methods have been employed for inferring model parameters as suggested by Foures *et al.* (2014). Parish and Duraisamy (2016) developed the field inversion and machine learning approach using Bayesian inference and machine learning to enhance RANS model predictions, achieving success in applications involving airfoils with separation (Singh *et al.* 2017). This approach was also applied in the framework of transition modeling in turbomachinery by Ferrero *et al.* (2020). Along these lines, the aim of this work is to improve the predictive capabilities of the SST RANS model by adding non-linear correction terms which increase the accuracy of the Boussinesq assumption. This is done by testing different formulations which allow to express the non-linear correction as a function of invariants. In order to improve the robustness of the model with respect to previous approaches, two different contributions are proposed: first of all, some simplified but robust relations between non-linear correction and invariants are discussed. Secondly, physical constraints have been introduced by means of penalizations during the training of the model. The proposed approach can be applied to both compressible and incompressible flows and represents an effort to increase the reliability of data-driven RANS models.

2. SST RANS model

The present work is focused on the SST k-ω model by Menter (1994). It is a two-equations model based on the eddy-viscosity approach which combines the best properties of the k-ω and k-ε models. The use of a k-ω formulation in the inner parts of the boundary layer makes the model

usable directly down to the solid wall through the viscous sublayer, so that the SST *k-ω* model can be used as a low-Reynolds turbulence model without additional damping functions. However, the *k-ω* model is very sensitive with respect to far field boundary conditions and this amplifies the uncertainty from the boundary conditions to the results. On the contrary, the *k-ε* model is not so sensitive to far field boundary conditions but it requires special treatment for integration close to solid walls. The SST formulation represents a continuous blending between *k-ω* and *k-ε* models, which uses *k-ω* close to the body and reverts to *k-ε* model in the free flow, avoiding the usual *k-ω* problems related to high-sensitivity to the inlet free-stream turbulence properties. The SST model is based on two transport equations for turbulent kinetic energy *k* and specific dissipation *ω*:

$$\frac{\partial(\rho k)}{\partial t}+\frac{\partial\left(\rho u_j k\right)}{\partial x_j}=P-\beta^*\rho\omega k+\frac{\partial}{\partial x_j}\left[(\mu+\sigma_k\mu_t)\frac{\partial k}{\partial x_j}\right]$$

$$\frac{\partial(\rho\omega)}{\partial t}+\frac{\partial\left(\rho u_j \omega\right)}{\partial x_j}=\frac{\gamma}{\mu_t}P-\beta\rho\omega^2+\frac{\partial}{\partial x_j}\left[(\mu+\sigma_\omega\mu_t)\frac{\partial \omega}{\partial x_j}\right]+2(1-F_1)\frac{\rho\sigma_{\omega 2}}{\omega}\frac{\partial k}{\partial x_j}\frac{\partial \omega}{\partial x_j}$$

Production term: $P=\tau_{ij}\frac{\partial u_i}{\partial x_j}$

Turbulent eddy viscosity: $\mu_t=\frac{\rho a_1 k}{\max(a_1\omega,\Omega F_2)}$

Where μ, μ_t, τ_{ij}, ρ represent dynamic viscosity, dynamic eddy viscosity, Reynolds stress tensor and density, respectively. The blending function F_1 allows to modify the behavior of the model from *k-ω* (close to solid walls) to *k-ε* (in the far field). The coefficients β, β^*, σ_k, σ_ω, γ and $\sigma_{\omega 2}$ assume the values suggested by Menter (1994).

In this framework, the Boussinesq assumption is used to evaluate the anisotropic part of the Reynolds stresses. That assumption links linearly the anisotropic part of the Reynolds stress tensor a_{ij} to the strain rate tensor S_{ij}

$$\tau_{ij}=a_{ij}-\frac{2}{3}\rho k\delta_{ij}=2\mu_t S_{ij}-\frac{2}{3}\rho k\delta_{ij} \tag{1}$$

where *k* is the turbulent energy and S_{ij} is the strain rate tensor defined as follows:

$$k=\frac{1}{2}\overline{u_i' u_j'}$$

$$S_{ij}=\frac{1}{2}\left(\frac{\partial u_i}{\partial x_j}+\frac{\partial u_j}{\partial x_i}\right)$$

The Boussinesq assumption plays a crucial role in this model and is widely used in RANS turbulence modeling because of its simplicity. However, extensive analysis based on high-fidelity data shows that the Boussinesq assumption introduces a significant error. Using DNS (or experimental) data, it is possible to quantify the error by examining the alignment between the strain rate tensor and the anisotropic part of the Reynolds stress tensor. It is possible to calculate the following quantity, which corresponds to a normalized scalar product between the anisotropic part of the Reynols stress tensor and the strain rate tensor:

$$\theta=\frac{a_{ij}S_{ij}}{\sqrt{a_{kl}a_{kl}S_{mn}S_{mn}}}$$

$$a_{ij}=\tau_{ij}+\frac{2}{3}\rho k\delta_{ij}$$

This indicator varies between -1 and 1. If θ is equal to 1, this means that the anisotropic part of the Reynolds stress tensor and the shear rate tensor are aligned and therefore that Boussinesq hypothesis is valid. If θ is equal to 0, this means that the two tensors are orthogonal, and if this value is equal to -1, then the two tensors are aligned, but in the opposite direction with respect to the Boussinesq hypothesis.

3. Non-linear correction

Pope (1975) introduced a nonlinear correction to address the discrepancy between the Reynolds tensor obtained through DNS/experiment and the one calculated using the Boussinesq approximation. This correction enhances the linear Boussinesq approximation by incorporating additional terms, creating a nonlinear constitutive stress-strain relationship. The model was based on the weak equilibrium hypothesis for the anisotropic part of the Reynolds tenso (a_{ij}): this hypothesis assumes that a_{ij} is approximately constant following a fluid particle. Pope (1975) identified the non-linear correction as a finite tensor polynomial by using dimensional analysis, imposing invariance under coordinate-transformation, and using physical arguments to limit the number of quantities which appear in the expression. The non-linear correction for general 3D flows is expressed by means of a tensor basis V^k and scalar invariants I_k

$$\tau_{ij} = 2\mu_t S_{ij} - \frac{2}{3}\rho k \delta_{ij} - \rho k \sum_{k=1}^{10} \alpha_k V_{ij}^k \tag{2}$$

V^k are basis functions formed from polynomials of non-dimensional strain rate $\tilde{S}_{ij} = \delta S_{ij}$ and rotation rate $\tilde{R}_{ij} = \delta R_{ij}$, where δ is the turbulent timescale. S_{ij} is the previously defined strain rate tensor and R_{ij} is the rotation rate tensor

$$R_{ij} = \frac{1}{2}\left(\frac{\partial u_i}{\partial x_j} - \frac{\partial u_j}{\partial x_i}\right) \tag{3}$$

$$V^1 = \tilde{S} \qquad V^6 = \tilde{R}^2\tilde{S} + \tilde{S}\tilde{R}^2 - \frac{2}{3}I\mathrm{Tr}\left(\tilde{S}\tilde{R}^2\right)$$

$$V^2 = \tilde{S}\tilde{R} - \tilde{R}\tilde{S} \qquad V^7 = \tilde{R}\tilde{S}\tilde{R}^2 - \tilde{R}^2\tilde{S}\tilde{R}$$

$$V^3 = \tilde{S}^2 - \frac{1}{3}I\mathrm{Tr}\left(\tilde{S}^2\right) \qquad V^8 = \tilde{S}\tilde{R}\tilde{S}^2 - \tilde{S}^2\tilde{R}\tilde{S}$$

$$V^4 = \tilde{R}^2 - \frac{1}{3}I\mathrm{Tr}\left(\tilde{R}^2\right) \qquad V^9 = \tilde{R}^2\tilde{S}^2 + \tilde{S}^2\tilde{R}^2 - \frac{2}{3}I\mathrm{Tr}\left(\tilde{S}^2\tilde{R}^2\right)$$

$$V^5 = \tilde{R}\tilde{S}^2 - \tilde{S}^2\tilde{R} \qquad V^{10} = \tilde{R}\tilde{S}^2\tilde{R}^2 - \tilde{R}^2\tilde{S}^2\tilde{R}$$

The coefficients α_k are functions of the non-dimensionnal invariants I_k formed by $\tilde{R}$ and $\tilde{S}$:

$I_1 = Tr(\tilde{S}^2), \quad I_2 = Tr(\tilde{R}^2), \quad I_3 = Tr(\tilde{S}^3), \quad I_4 = Tr(\tilde{R}^2\tilde{S}), \quad I_5 = Tr(\tilde{R}^2\tilde{S}^2)$

In its original work, Pope suggested two possible ways to evaluate δ as:

$$\delta_\omega = \frac{k}{\epsilon} = \frac{1}{\omega} \quad \text{or} \quad \delta_v = \left(\frac{\partial u_i}{\partial x_j}\frac{\partial u_i}{\partial x_j}\right)^{-1/2}$$

where the turbulence dissipation ϵ and the specific dissipation ω are related by the following expression: $\omega = \epsilon/k$. In this work, the first approach $\delta = \delta_\omega$ is adopted, following the recommendation by Pope (1975). A possible motivation to choose δ_ω instead of δ_v is that in a turbulence homogeneous flow, δ_ω is defined while δ_v is not.

Finally, Pope (1975) showed than for 2D flows it is possible to reduce the tensor basis which appears in Eq. (2) to the first three terms and the coefficients α_k can be computed as a function of the first two invariants.

4. Realizability conditions

In order to obtain a physically realizable model, it is important to impose some constraints to the Reynolds stress tensor. The Reynolds stress tensor is by definition symmetrical semi-definite negative.

$$\begin{cases} -\overline{\rho u_i'^2} \leq 0 \\ \left(\overline{\rho u_i' u_j'}\right)^2 \leq \overline{\rho u_i'^2}\,\overline{\rho u_j'^2} \end{cases} \tag{4}$$

The first inequality is referred to as the linear or diagonal constraint. Since the Reynolds stress tensor is negative semi-definite, the diagonal elements must be less than or equal to zero. In addition, each element of the diagonal should be greater than or equal to the trace of the Reynolds stress tensor. Otherwise, this would mean that at least one element of the diagonal would have to be positive. The second inequality is known as the quadratic constraint or the Cauchy-Schwarz inequality. This condition can be expressed as the requirement that the square of the covariance must not exceed the product of the variances. Another way of considering these realizability conditions is to look at the eigenvalues of the Reynolds stress tensor, which must all be negative.
These conditions are not necessarily met by the k-omega SST model and by the non-linear corrections that are investigated in the present work. This aspect will be taken into account by introducing these constraints in the following.

5. Non-linear model training on DNS data

The first step of the proposed methodology is focused on the analysis of high-fidelity data (from DNS or experiments) to identify the coefficients of the non-linear correction reported in Eq. (2). Ideally, the coefficients α_1 should be expressed as a function of the invariants: Sandberg and Michelassi (2019) identified this relationship by means of gene expression programming and they proposed to consider a truncated expansion in which only the leading terms of the function are evaluated and only the first two invariants are considered. During the initial phase of this work, the use of neural networks was investigated as a possible way to obtain the coefficients α_k as a function of local flow features. However, the coefficients produced by these networks exhibited strong oscillations, resulting in instabilities when implemented in the RANS CFD code. For this reason, we did not use artificial neural networks, but an alternative strategy was investigated.

In a preliminary step of this work, the non-linear models provided by Zhao *et al.* (2020) was tested on the periodic hill test case by Xiao *et al.* (2020): the results showed that the coefficients

α_k remained almost constant through the domain, with small variations induced by the invariants. For this reason, in the present work the possibility of using constant coefficients α_k is investigated. The use of constant values for α_k significantly improves the robustness of the subsequent RANS simulation since it avoids the development of non-physical values during transients in predictive simulations. The coefficients α_k are obtained by solving an optimization problem in which the goal function is represented by the L2 norm error between the Reynolds stresses computed by the nonlinear model applied to the DNS field and the Reynolds stresses obtained from the DNS. Furthermore, the goal function is augmented by a penalization term which measures the violation of the realizability conditions. As a result, the considered goal function is defined as

$$f(\alpha_1, \alpha_2, \alpha_3) = |\tau^{DNS} - \tau^{RANS}| + \eta g \tag{5}$$

where

$$\begin{cases} \tau_{ij}^{DNS} = -\rho\overline{u_i' u_j'} \\ \tau_{ij}^{RANS} = 2\mu_t S_{ij} - \frac{2}{3}\rho k \delta_{ij} - \rho k \sum_{k=1}^{3} \alpha_k V_{ij}^k \\ g = \sum_{i=1}^{2} \max(\lambda_i, 0)^2\,, \quad \lambda = \text{eigen value of } \tau^{RANS} \\ \eta = 1000 \end{cases}$$

The optimisation problem is solved using the Broyden-Fletcher-Goldfarb-Shanno (BFGS) method described by Broyden (1969). The value of the penalization constant η can be identified by a trial-and-error procedure which aims to make the error term and the penalization term of the same order of magnitude.

Furthermore, a potentially more accurate correction is investigated by assuming that the coefficients α_k are linear functions of the first two invariants. In this case, the optimization problem is solved in order to find nine coefficients, $\alpha_k^i, (1 \le k \le 3, 0 \le i \le 2)$.

$$f(\alpha_1, \alpha_2, \alpha_3) = |\tau^{DNS} - \tau^{RANS}| + \eta g \tag{6}$$

$$\begin{cases} \alpha_i = \left(\alpha_i^0, \alpha_i^1, \alpha_i^2\right) \\ \tau_{ij}^{DNS} = -\rho\overline{u_i' u_j'} \\ \tau_{ij}^{RANS} = 2\mu_t S_{ij} - \frac{2}{3}\rho k \delta_{ij} - \rho k \sum_{k=1}^{3} \left(\alpha_k^0 + \alpha_k^1 I_1 + \alpha_k^2 I_2\right) V_{ij}^k \\ g = \sum_{i=1}^{2} \max(\lambda_i, 0)^2\,, \quad \lambda = \text{eigen value of } \tau^{RANS} \\ \eta = 1000 \end{cases}$$

6. Characteristic time correction in RANS simulations

The non-linear model obtained by training on the DNS data can then be implemented and tested in the RANS solver. Some preliminary tests on the same geometries used for the training of the non-linear model showed a significant effect of the non-linear terms on the RANS results: in particular, the non-linear terms introduce an excessive correction as will be clarified in Section 8.2 for the periodic hill test case. This can be explained by the fact that the non-linear correction was

trained on the averaged DNS field which cannot be exactly reproduced by the RANS simulation. In particular, there is a significant uncertainty on the time scale $\delta = 1/\omega$ used to normalize the tensor basis. This uncertainty lies in the very definition of the specific dissipation: ω is related to turbulence dissipation ϵ by means of dimensional analysis. However, dimensional analysis does not provide any scale factor.

For this reason, the turbulence characteristic time obtained by the DNS and the turbulence characteristic time estimated from the field in the RANS can be quite different. In order to solve this problem, Parneix *et al.* (1998) proposed to integrate the RANS ω equation up to steady state while keeping all the other flow variables frozen to the average values provided by the DNS. The resulting field can be used in the training to estimate a turbulence characteristic time which will be coherent with the RANS model in which the non-linear terms will be used. In the present work, this procedure is avoided and substituted by an alternative approach. In particular, the evaluation of the turbulence characteristic time $\tau = 1/\omega$ is improved by introducing a correction factor computed through an Artificial Neural Network K_{ANN}

$$\tilde{\tau} = \tau K_{ANN}(x_1, x_2) \tag{7}$$

where the following inputs are considered

$$x_1 = \min\left(2, \rho\sqrt{k}d/\mu\right), \qquad x_2 = \frac{\delta_v}{\delta_v + \delta_\omega + 10^{-10}} \tag{8}$$

The first input is the wall distance-based Reynolds number which is limited to two according to Wang *et al.* (2017). The second input represents a measure of the discrepancy between two alternative definitions of the characteristic time. Both inputs are defined in a limited range. The ANN architecture was chosen after some preliminary investigations: a very small ANN with two inputs and one hidden layer with two neurons is considered. The weights and biases of the ANN are computed through an optimization problem which requires to introduce the RANS solver in the loop. In particular, an optimization problem is defined by considering the following goal function

$$f = \int_{CS} (u_{RANS} - u_{DNS})^2 \, dy + \varphi Y \tag{9}$$

where u_{RANS} and u_{DNS} are the velocity profile in some control stations CS in the computational domain. The penalization function Y is computed as an integral of the realizability error E_{real} on the entire domain Ω

$$Y = \int_\Omega E_{real} d\Omega \tag{10}$$

$$E_{real} = \frac{|\tau - \tilde{\tau}|}{\rho_b u_b^2} \tag{11}$$

where τ represents the Reynolds stress tensor computed by the RANS model and $\tilde{\tau}$ represents its limited version which satisfies the realizability conditions. The Frobenius norm is applied to the difference between the two tensors and the results is normalized with respect to a reference pressure obtained from bulk density ρ_b and bulk velocity u_b (the approach will be applied to a channel flow and so the bulk values are chosen). The tensor $\tilde{\tau}$ is computed in the following way

$$\tilde{\tau}_{ij} = \min\left(0, \tau_{ij}\right) \qquad \text{if} \quad i = j \tag{12}$$

$$\tilde{\tau}_{ij} = \begin{cases} sign(\tau_{ij})\sqrt{\tilde{\tau}_{ij}\tilde{\tau}_{ij}} & if\ {\tau_{ij}}^2 > \tilde{\tau}_{ii}\tilde{\tau}_{jj} \text{ and } i \neq j \\ \tau_{ij} & if\ {\tau_{ij}}^2 \leq \tilde{\tau}_{ii}\tilde{\tau}_{jj} \text{ and } i \neq j \end{cases} \tag{13}$$

The penalization constant φ is chosen in order to make the error on the velocity profile and the penalization function Y of the same order of magnitude. A possible choice is to evaluate these two terms on the solution obtained at the beginning of the optimization process and to evaluate the constant φ as the ratio between these two terms

$$\varphi_0 = \frac{\left[\int_{CS}(u_{RANS} - u_{DNS})^2\, dy\right]_0}{Y_0} \tag{14}$$

The optimization problem is solved by a simple gradient descent approach and the iterations are arrested when the gradient magnitude becomes negligible. It is important to remember that including the RANS in the optimization loop helps in improving the robustness of the model since this approach can put in evidence any numerical instability or stiffness in the non-linear correction.

Furthermore, the optimization procedure will improve the prediction by including in K_{ANN} the corrections for different error sources, not just for the turbulence characteristic time. Finally, it is important to observe that performing the optimization directly on the coefficients of the ANN allows to obtain a data-driven model which can be immediately employed in a RANS simulation since the RANS was included in the optimization loop and the obtained correction is defined as a function of the chosen flow features: this property is not guaranteed in the field inversion and machine learning approach because it could be impossible to describe the correction field provided by field inversion as a function of local flow features. The approach used in the present work is in line with the strategy proposed by Ferrero *et al.* (2019) where an optimization was performed on the weights of an ANN to identify a correlation for a closure model.

7. RANS solver

In the following the results provided by the RANS equations with different closure models will be discussed. The governing equations are discretized by means of the finite volume approach implemented in a research code for compressible turbulent flows. The flow field considered in this work is incompressible (periodic hill test case) or with negligible compressibility (NASA hump test case). The incompressible flow is simulated by setting the Mach number to 0.1. This value makes the effects of compressibility negligible without the need to introduce preconditioning for low Mach number flows. The domain is discretized through a structured mesh obtained by the Gmsh opensource tool described by Geuzaine and Remacle (2009). The parallelization is managed through the DMPlex class of the PETSc library described in the PETSc User manual (2023) and by Balay *et al.* (1997): the library is available from the PETSc website (2023). The spatial discretization is second order accurate and it is limited following the approach of Barth and Jespersen (1989). Convective fluxes are computed by means of a hybrid approach proposed by Ferrero and D'Ambrosio (2020) which performs a blending between the local Lax-Friedrichs or Rusanov flux (1962) and an upwind flux based on an approximate solution of a Riemann problem described by Pandolfi (1984). The gradients required to compute diffusive fluxes are obtained by means of the weighted least squares approach. The governing equations are integrated in time by means of a linearized implicit Euler scheme: the resulting linear system is solved by the GMRES

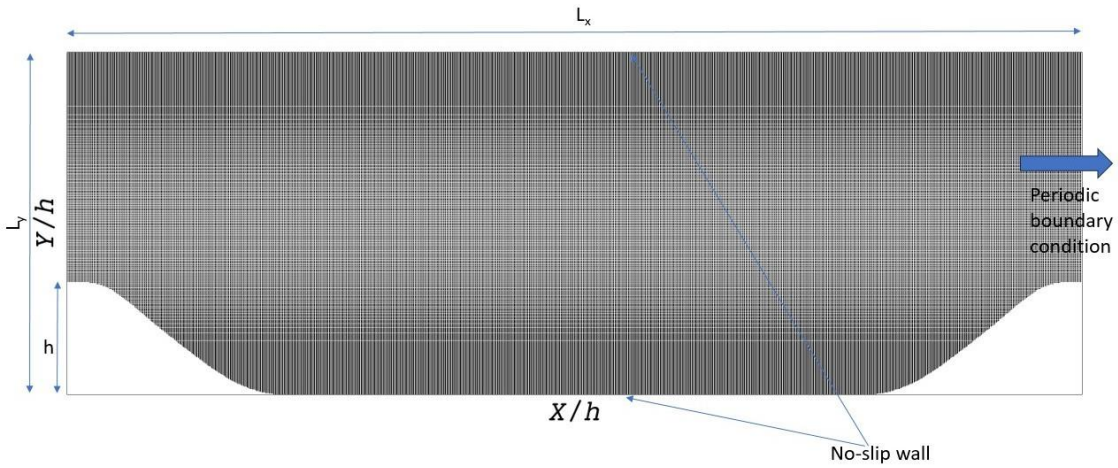

Fig. 1 Computational domain for the baseline geometry

algorithm with the Additive-Schwarz preconditioner.

8. Flow on a periodic hill

8.1 Preliminary analysis and training on DNS data

The flow over a periodic hill is a reference test case for evaluating the predictive capability of RANS models on separated flows. This configuration is characterised by complex flow features which include separation on the curved surface, reattachment on the flat surface and an unstable shear layer around the main recirculation bubble. Furthermore, high-fidelity results obtained through DNS are available for this case. Recently, Xiao *et al.* (2020) carried out 27 DNS on this test case by varying several geometric parameters while keeping the Reynolds number fixed at 5600. In particular, they varied the geometry by scaling the width of the hill by a coefficient α=0.5, 0.8, 1.0 (baseline), 1.2, 1.5 and 3.0 while setting the length of the flat section equal to ξ= 2.142, 5.142 (baseline) or 8.142. This geometry variability allows to observe incipiently separated, mildly separated, and vastly separated flow configurations.

The baseline periodic-hill geometry is represented as piecewise third-order polynomial functions. It represents a channel with a curved hill of height h and periodic streamwise boundary conditions, as can be seen in Fig. 1. The channel height is L_y=3.035 h and the horizontal length is parametrized by α as $L_x = (3.858\alpha + \xi)h$. Furthermore, three different height are considered $L_y/h = 2.024, 3.035, 4.048$. Non-slip boundary conditions are applied at the walls. The flow in the streamwise direction is driven by a uniform body force, which is implemented as a forcing term in the *x*-momentum equation to ensure the specified bulk Reynolds number:

$$Re_b = \frac{u_b h}{\nu} = 5600 \qquad \text{with} \qquad u_b = \frac{1}{2.035h}\int_h^{3.035h} u_1(y)dy$$

Since the spanwise direction is homogeneous then the mean flow is two-dimensional. The database provided by Xiao *et al.* (2020) includes:

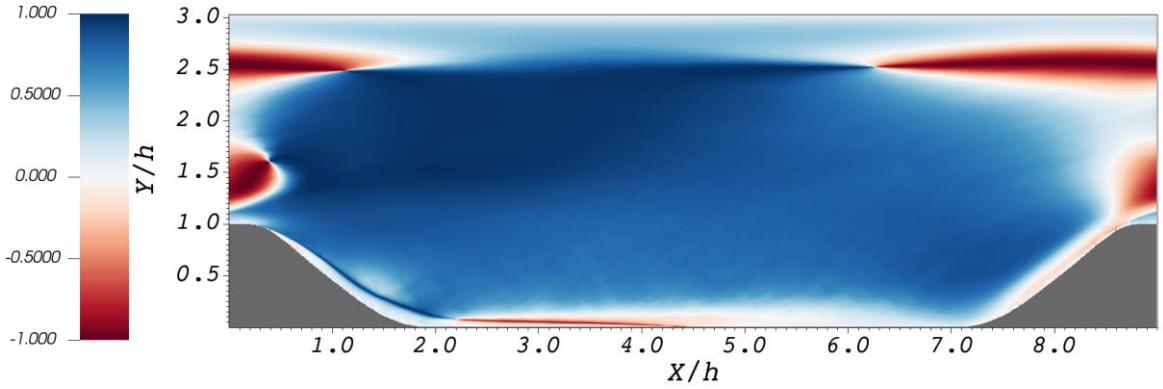

Fig. 2 Alignment of anisotropic part of Reynolds stress tensor with the strain rate tensor (θ) using DNS data of the flow over a periodic hill at *Re*=5600 from Xiao *et al.* (2020)

- Mean pressure field
- Mean velocities fields
- Second order statistics of velocities
- Mean dissipation rate

First of all, a RANS simulation with the standard SST model is performed on the baseline geometry. The simulation is performed on a structured mesh with 512×256 cells: this mesh resolution was chosen after a grid refinement study and it is expected to provide grid converged results. The same mesh resolution is adopted for all the simulations reported in this work. The steady solution is obtained by means of time-marching with a linearized implicit Euler scheme: the CFL number, initially set to 1, is increased up to 1000 during the numerical transient.

The obtained Reynolds stress tensor is compared to the DNS data by Xiao *et al.* (2020) in terms of the alignment sensor θ, defined by Eq. (2). The results of the comparison are reported in Fig. 2 which shows the presence of large portions of the domain in which the Boussinesq assumption is not valid.

This preliminary check motivates the introduction of the non-linear correction. The approach described in Section 3 is applied to the test case. First of all, a subset of the DNS data provided by Xiao *et al.* (2020) are used to identify the coefficients of the non-linear correction reported in Eq. (2). When the penalization term on the realizability conditions is deactivated (e.g., η=0) the following coefficients are obtained

$$\alpha_1 = -8.484, \qquad \alpha_2 = -5.956, \qquad \alpha_3 = 0.021 \tag{15}$$

When the penalization term is active (η=1000) the following coefficients are obtained

$$\alpha_1 = -5.456, \qquad \alpha_2 = -19.999, \qquad \alpha_3 = 19.999 \tag{16}$$

In this last case, the optimization problem seems to have several local minimum and, for this reason, a genetic algorithm described by Holland (1992) is adopted to minimise the goal function. This method provided better quality results than other classic optimization algorithms tested in this study (Broyden 1969, PowellPowell 1964, Nelder-MeadNelder and Mead 1965).

Finally, the non-linear correction with coefficients expressed as linear functions of the invariants I_1 and I_2 (see Eq. (6)) is evaluated. Also in this case the use of a genetic algorithm helps in avoiding local minima. The following coefficients are obtained

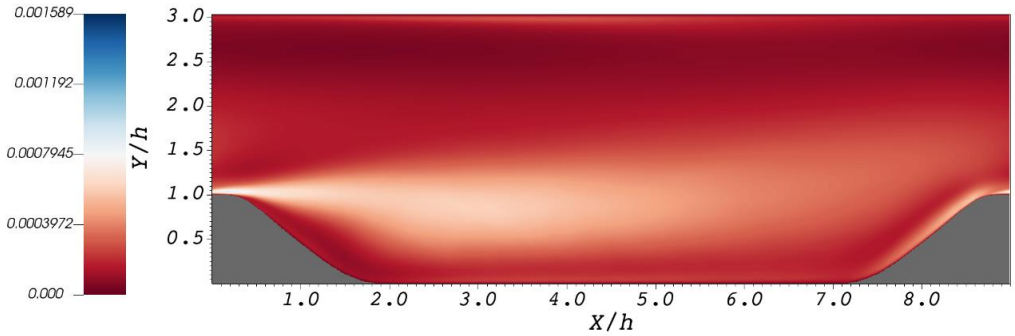

(a) Boussinesq assumption

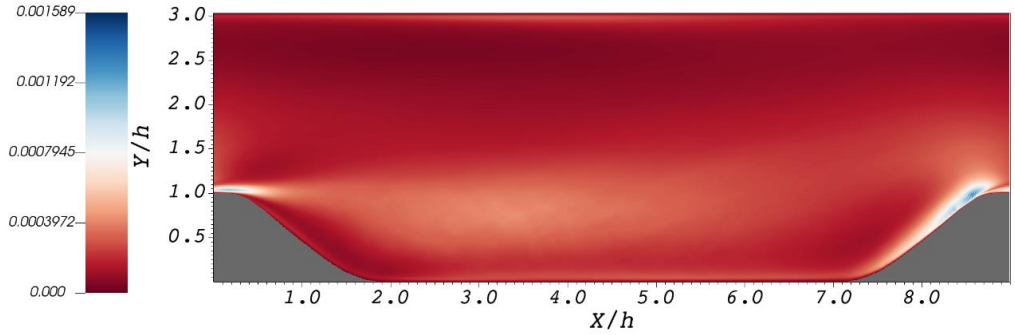

(b) Boussinesq assumption corrected with constant α_k found without the penalization term

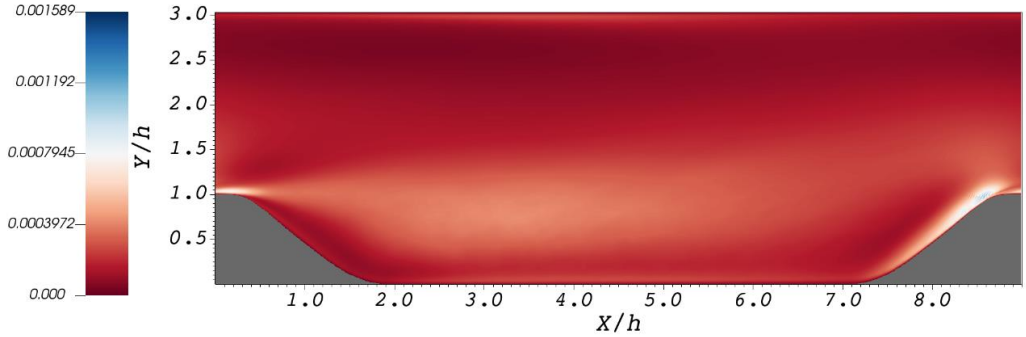

(c) Boussinesq assumption corrected with constant α_k found with the penalization term

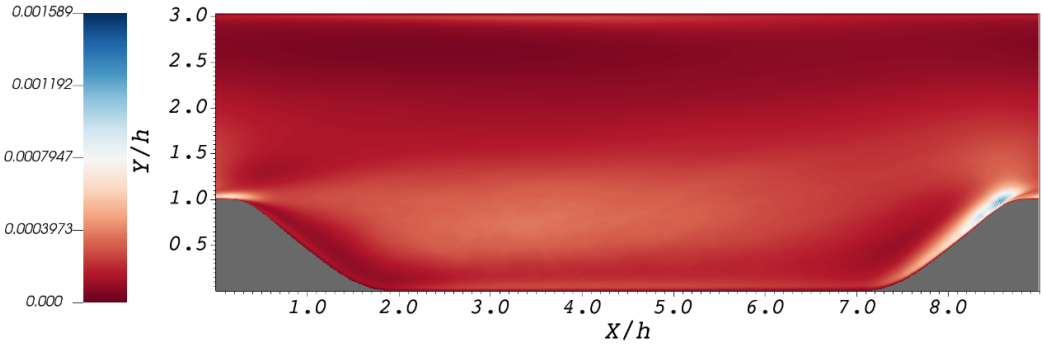

(d) Boussinesq assumption corrected with linear $\alpha_k(I_1, I_2)$ found with the penalization term

Fig. 3 Frobenius norm of the error on the Reynolds stress tensor

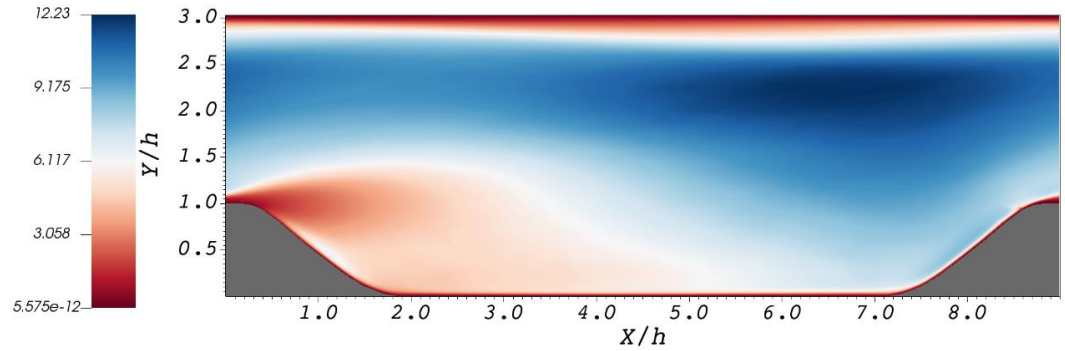

(a) DNS results

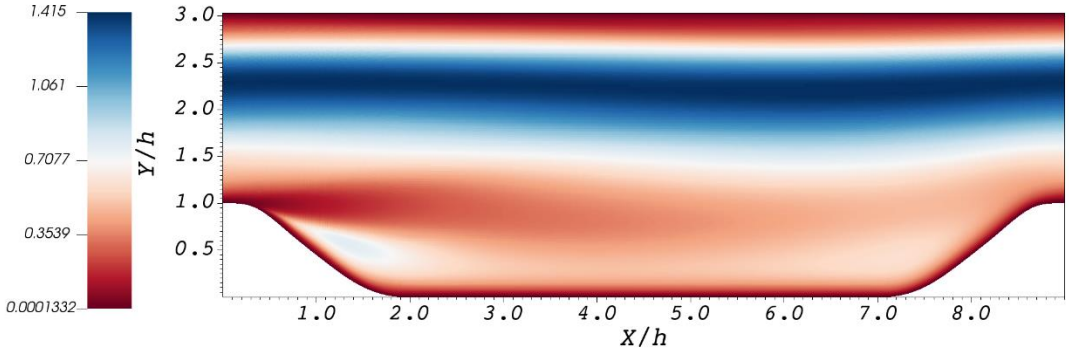

(b) RANS SST results

Fig. 4 Characteristic time field obtained from DNS and RANS SST simulations on baseline geometry

$$\begin{cases} \alpha_1 = (-6.568, -18.128, -93.892) \\ \alpha_2 = (-34.643, 15.834, 49.487) \\ \alpha_3 = (53.297, 67.308, 8.101) \end{cases} \tag{17}$$

The performance of the different models is evaluated by computing the Frobenius norm of the difference between the Reynolds stress tensor provided by the DNS and the one computed from the RANS. This comparison is reported in Fig. 3: it is possible to observe that, when the non-linear correction is active, the average error is reduced with respect to the original SST model described in Section 2. However, there is a limited portion of the domain near the exit where the non-linear correction introduces an error larger than SST and so the norm-infinite error is larger with the non-linear correction. This could be related to the fact that the optimization procedure used for finding the coefficients of the non-linear correction is driven by the L2 norm of the error and not the L-∞ norm.

8.2 Characteristic time correction with RANS in the optimization loop

The characteristic time, computed as the inverse of the specific dissipation rate, is evaluated from the DNS data and from a RANS simulation with the original SST model described in Section 2. The characteristic time field, normalized with respect to bulk velocity and height of the hill, is reported in Fig. 4 for DNS and SST. The results show clearly that the two approaches lead to

Table 1 Properties of investigated non-linear corrections

MODEL	$\tilde{\tau}/\tau$	η	β	Coefficients α_k
A	1	0	-	Constant (Eq. (15))
B	$k_{ANN}(x_1, x_2)$	0	β_0	Constant (Eq. (15))
C	$k_{ANN}(x_1, x_2)$	1000	β_0	Constant (Eq. (15))
D	$k_{ANN}(x_1, x_2)$	1000	β_0	$\alpha_k = \alpha_k^0 + \alpha_k^1 I_1 + \alpha_k^2 I_2$

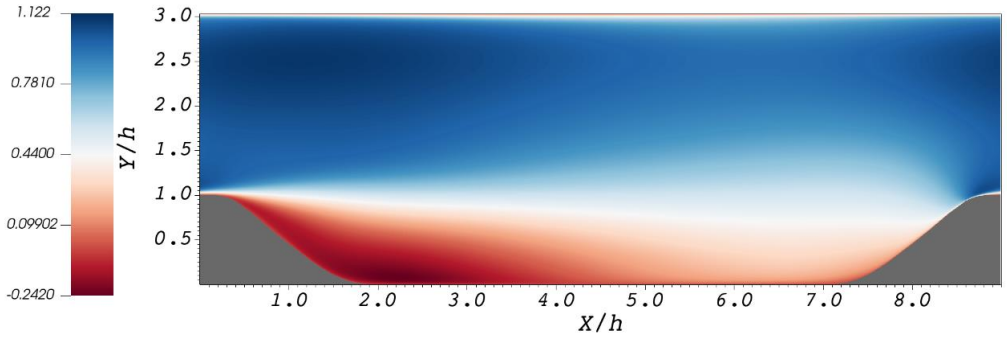

(a) DNS data

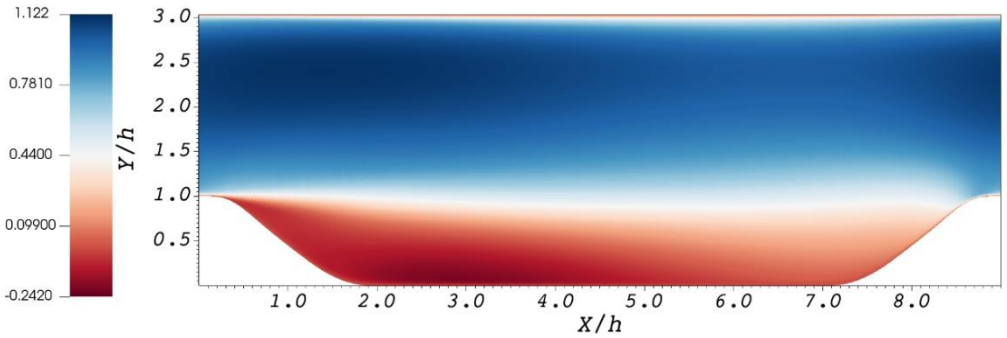

(b) RANS SST results

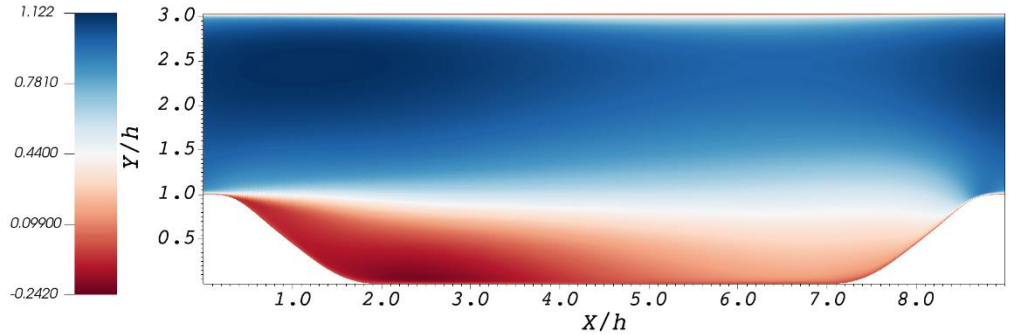

(c) RANS SST+model D results

Fig. 5 Axial velocity field

significant differences: this is a critical point since the characteristic time is required to normalize the strain rate and rotation rate tensors on which the non-linear correction is based. The flow field

Table 2 Velocity error on the profiles at *x/h*=2 and *x/h*=4 for the different models for baseline geometry

MODEL	ε at *x/h*=2	ε at *x/h*=4
SST	9.80e-03	2.94e-02
A	5.43e-03	1.25e-02
B	2.07e-03	3.19e-03
C	2.04e-03	2.76e-03
D	2.52e-03	3.97e-03

on the baseline geometry is computed with different models and compared with the DNS results. In particular, the non-linear corrections listed in Table 1 are considered. The model A is obtained by adding the nonlinear correction with constant coefficients α_k obtained from the DNS data without the penalization for the realizability conditions: it does not include any correction on the characteristic time. The model B uses the same α_k coefficients of model A but the characteristic time is corrected by an ANN. The model C is based on constant coefficients α_k obtained by training on the DNS data with a penalization on the violation of realizability conditions: it includes an ANN for the correction of the characteristic time. Finally, the model D is based on coefficients α_k which are linear functions of the invariants: realizability conditions are taken into account by means of penalization both in the DNS training and in the identification of the ANN correction for the characteristic time.

The axial velocity field (normalized with bulk velocity) obtained by the DNS, the original SST model and the model D is reported in Fig. 5. It is possible to observe that the original SST model tends to overpredict the size of the recirculation region. The turbulent kinetic energy normalized with the square of the bulk velocity is reported in Fig. 6 for the same models. A more quantitative comparison can be performed by plotting the axial velocity profile in some control sections. In particular, the axial velocity profiles at *x/h*=2 and *x/h*=4 are reported in Figs. 7 and 8. It is possible to observe that the model A, which was trained on the DNS data but does not include the correction on the characteristic time, tends to underpredict the velocity profile.

On the contrary, the models B, C and D, which include the RANS characteristic time correction, provide similar results which are in better agreement with respect to the DNS data. The Table 2 shows the velocity errors of the different models at *x/h*=2 and *x/h*=4.

The L-2 norm of the velocity error is computed as follows

$$\epsilon = \int_{CS} (U_{DNS} - U_{model})^2 dy \tag{18}$$

Finally, a measure of the error on the realizability conditions is reported in Fig. 9. The error is computed according to Eq. (11). It is important to observe that the original SST model introduces negligible violations on the realizability conditions in this test case: they are localized in a very thin layer close to the wall which cannot be observed from the picture. However, if a non-linear correction is applied to the Boussinesq assumption without any control on the realizability conditions then it is possible to achieve large violations, as shown by the results provided by model A. For this reason, it is important to introduce a penalization term on the realizability conditions as shown by the results provided by models C and D which are characterised by small violations of the realizability conditions but provide a better prediction of the velocity profile with respect to the original SST model, as shown in the following. It is interesting to see that the non-

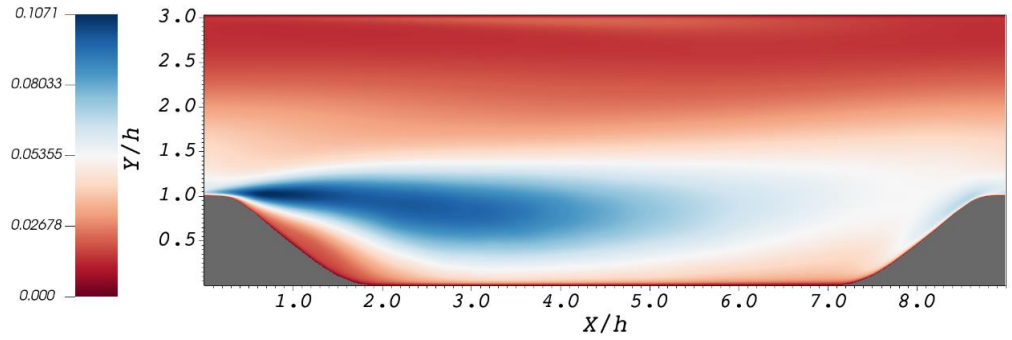

(a) DNS data

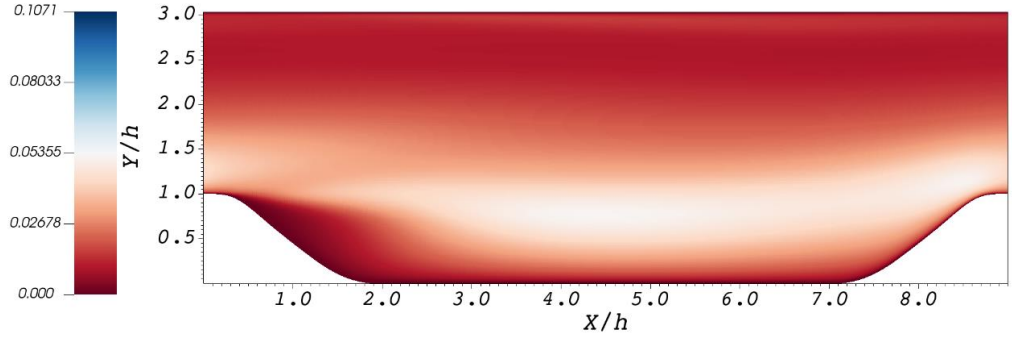

(b) RANS SST results

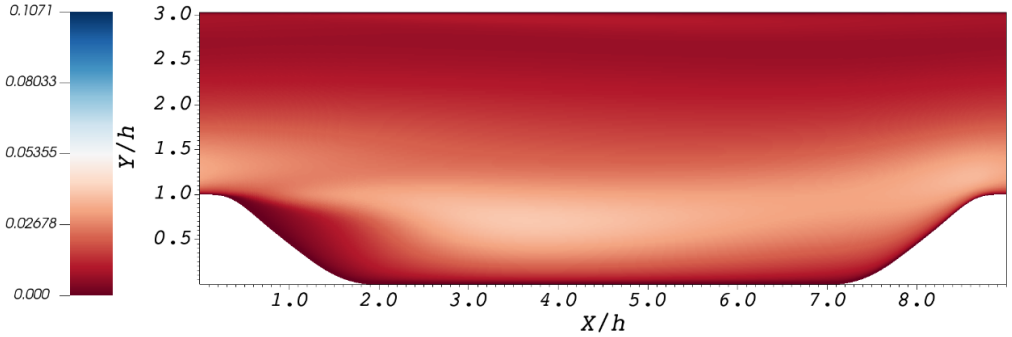

(c) RANS SST+model D results

Fig. 6 Turbulent kinetic energy normalized with the square of the bulk velocity

linear model D trained on the DNS and with the characteristic time correction provided by the ANN obtains a good performance, predicting a velocity profile which is closer to DNS data with respect to the original SST model.

8.3 Predictions on different hill geometries

The neural network used to correct the characteristic time was trained on the baseline geometry. In this Section, predictive results on other hill geometries will be reported. As done previously, DNS, RANS SST and model D are compared looking to the axial velocity profile at

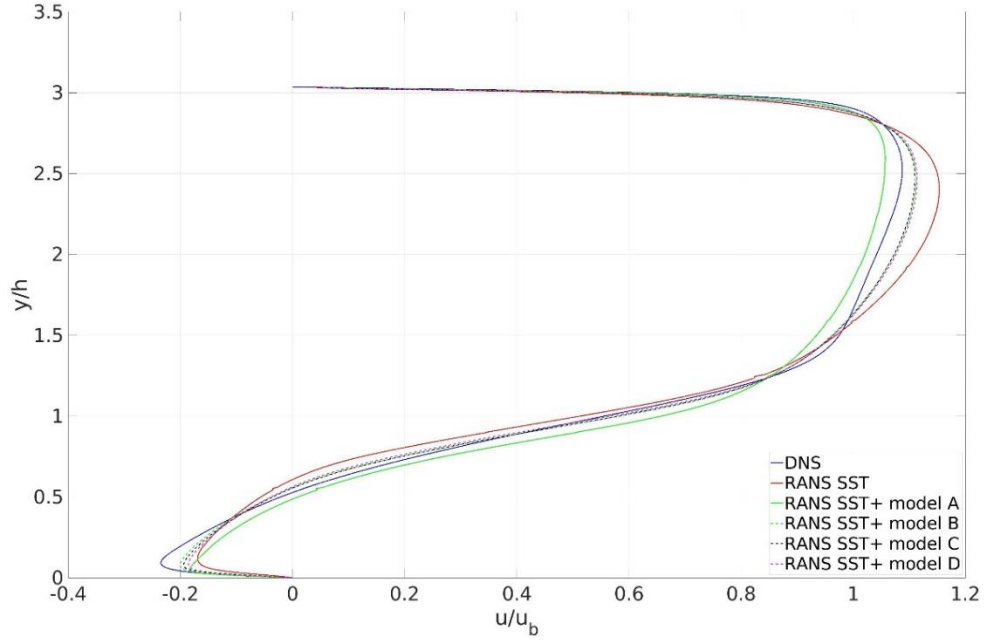

Fig. 7 Axial velocity profile at x/h=2 for baseline geometry

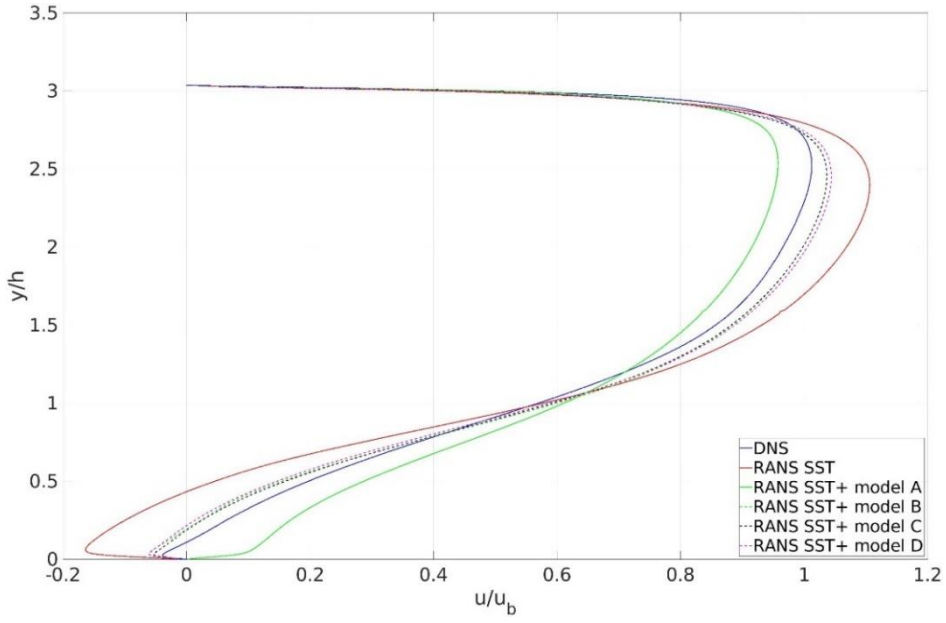

Fig. 8 Axial velocity profile at x/h=4 for baseline geometry

two control stations, x/h=2 and x/h=4. The first test is performed on the geometry corresponding to the value α=1.5, β=5.142 and Ly/h=2.024 (this configuration will be denoted in the following as Test 1). The velocity profile provided by the different models is reported on Fig. 10 for the control section x/h=2 and Fig. 11 for the control section x/h=4. These two Figures show that the model D

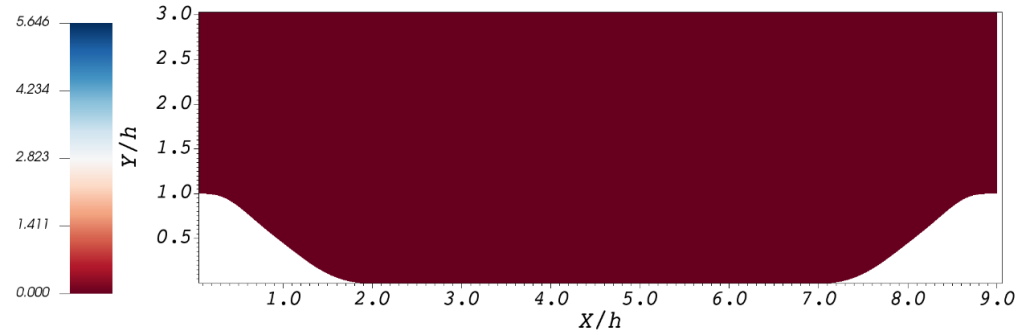

(a) SST

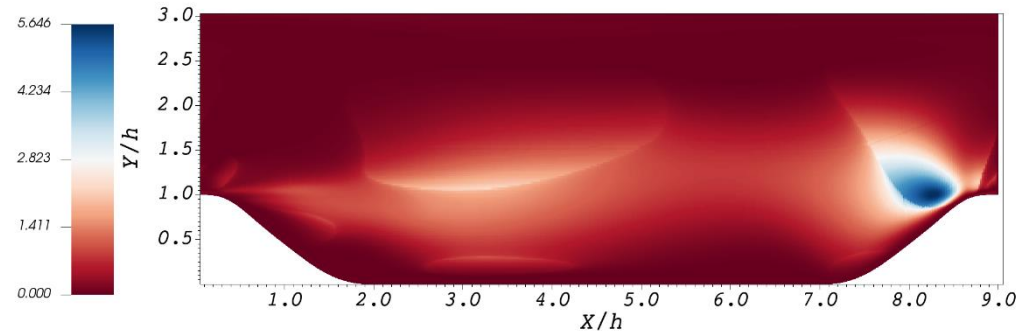

(b) Model A

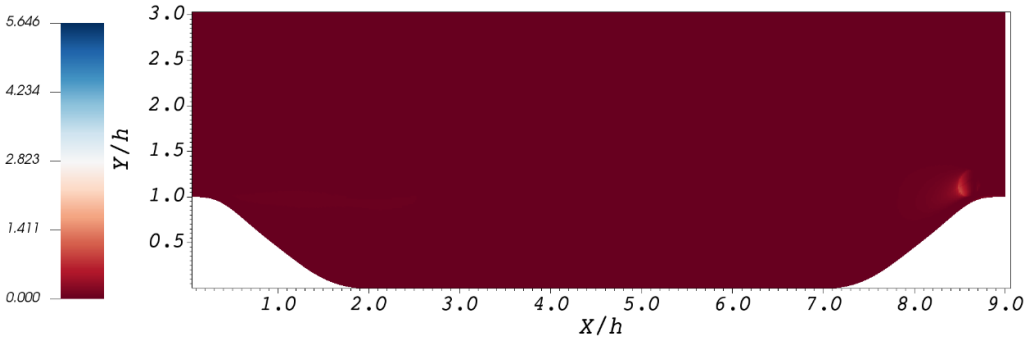

(c) Model C

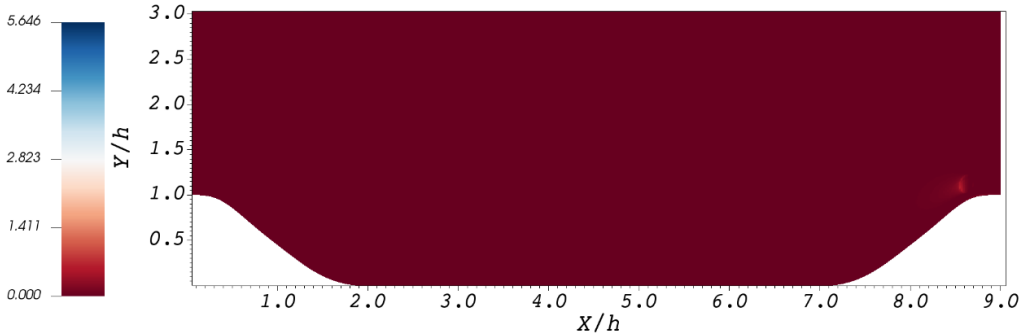

(d) Model D

Fig. 9 Error on realizability conditions on baseline geometry

Table 3 L-2 norm velocity error for SST model and SST+model D on Test 1 geometry

MODEL	ε at x/h=2	ε at x/h=4
SST	2.38e-02	8.07e-02
D	3.97e-02	1.70e-02

Table 4 L-2 norm velocity error for SST model and SST+model D on Test 2 geometry

MODEL	ε at x/h=2	ε at x/h=4
SST	2.22e-01	2.98e-01
D	1.79e-01	1.87e-01

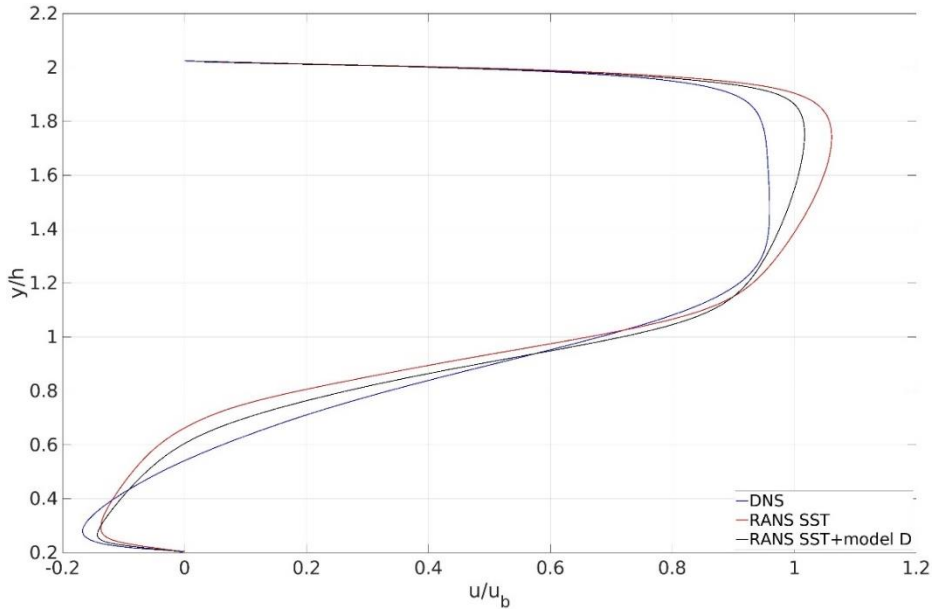

Fig. 10 Axial velocity profile at x/h=2 for Test 1 geometry

is a clear improvement on the RANS model. In order to perform a more quantitative comparison, the Table 3 groups together the errors calculated on this test case.

The second test (Test 2 in the following) is performed on a geometry corresponding to the value α=1.5, β=8.142 and Ly/h=3.036. The velocity profile of the three models used on this geometry is reported on the Fig. 12 for the control point x/h=2 and the Fig. 13 for the control point x/h=4. Both graphs show an improvement when model D is used. However, this improvement is less significant than in the baseline geometry and in test 1. The error on the velocity profile is reported in Table 4.

9. Prediction on NASA hump test case

The original SST model and the model D are tested on the 2D NASA wall-mounted hump separated flow validation case described by Greenblatt *et al.* (2006). This test case was introduced

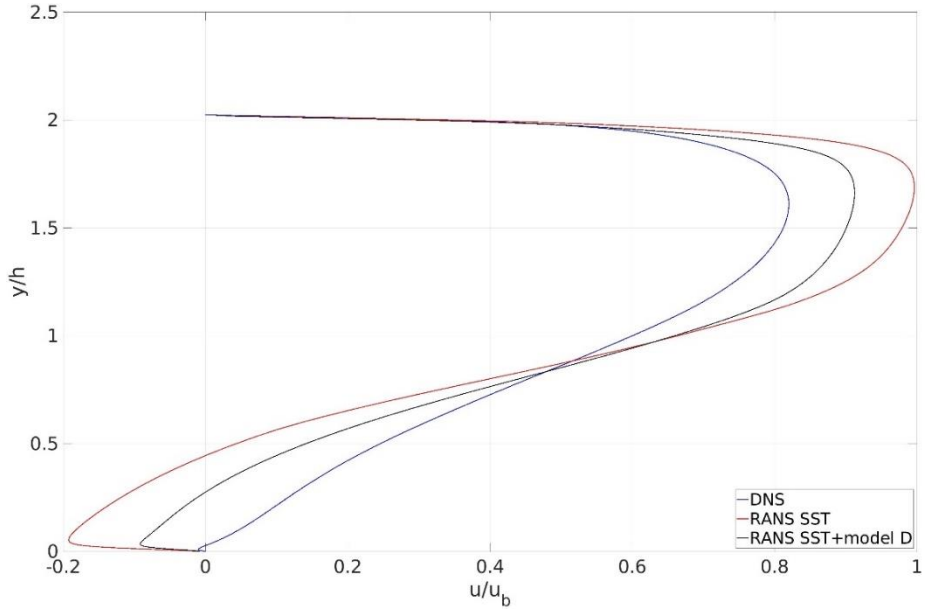

Fig. 11 Axial velocity profile at *x/h*=4 for Test 1 geometry

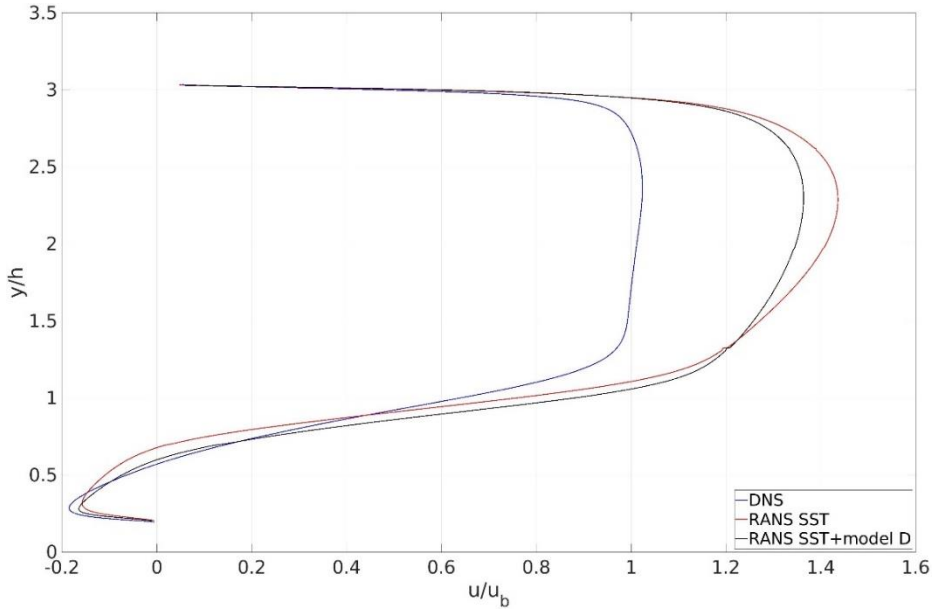

Fig. 12 Axial velocity profile at *x/h*=2 for Test 2 geometry

to assess the ability of turbulence models to predict 2-D separation from a smooth body and subsequent reattachment. The working conditions and geometry are reported on the NASA Turbulence Modeling Resource website by Rumsey *et al.* (2010). The far field Mach number is 0.1 and the Reynolds number based on the chord of the hump is 936000. The original experimental setup included a plenum which was used for flow control. The present work is focused on the case

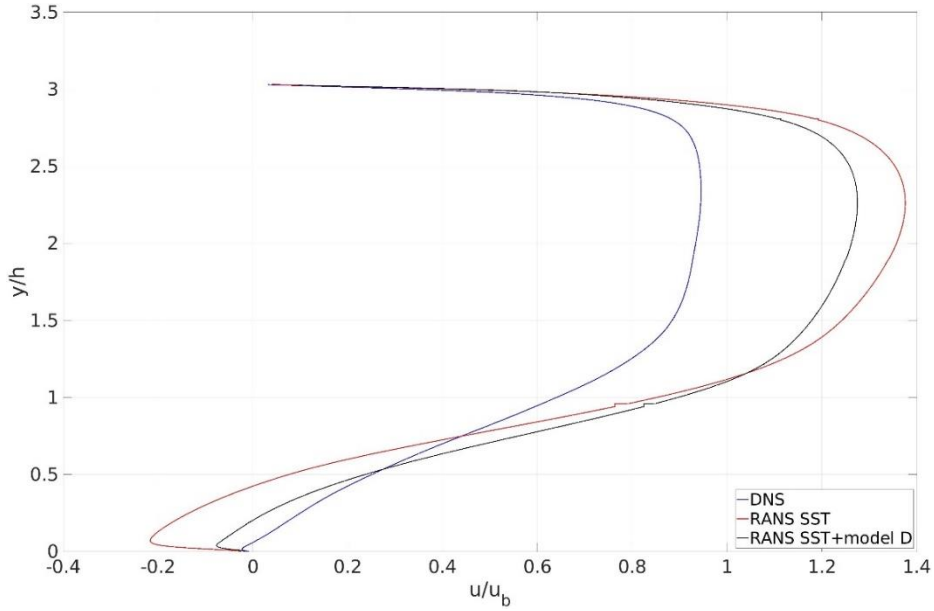

Fig. 13 Axial velocity profile at *x/h*=4 for Test 2 geometry

Table 5 Prediction of reattachment position in NASA hump test case

SOURCE	Reattachment position (x/c)
Experiment	1.10
RANS SST	1.26
RANS SST+ Model D	1.10

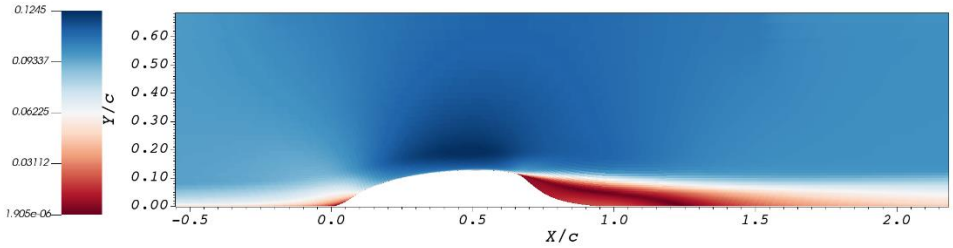

Fig. 14 Detail of the Mach number field for the NASA hump case with SST model

without flow control and so the plenum is not included in the computational domain. The simulations are performed on a structured mesh with 409×109 cells obtained from the NASA Turbulence Modeling Resource website. The Mach field obtained with the SST model is reported in Fig. 14 which clearly shows the large separation and the reattachment. The Mach field allows to perform only a qualitative comparison and it is difficult to evaluate the quality of the prediction from this picture. A more objective comparison between SST and SST+model D is performed by comparing the wall pressure coefficient provided by these two models with the experimental results, as reported in Fig. 15: the results suggest that model D performs better than the original SST model. This is confirmed by the prediction of the reattachment position which is reported in

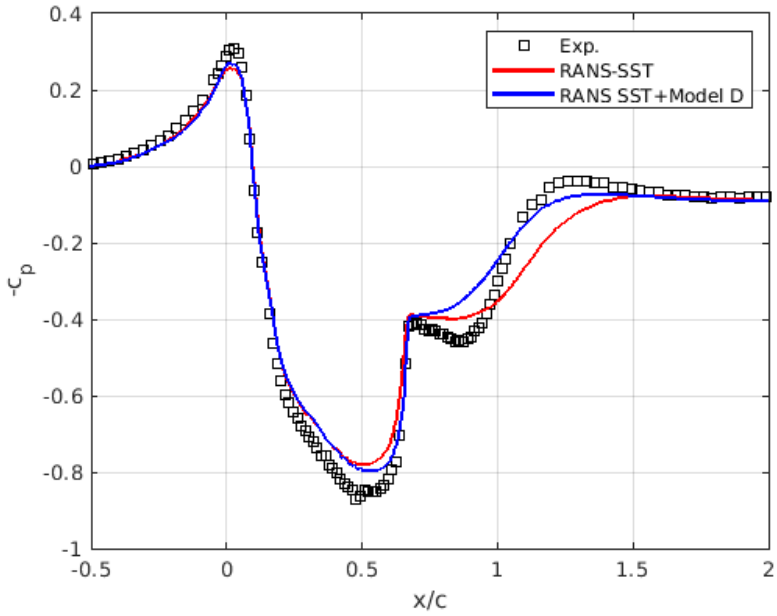

Fig. 15 Wall pressure coefficient on the NASA hump case

Table 5: the axial position x is normalized with respect to the axial length of the hump c. The prediction of the reattachment position, which is identified by a sign change in the wall friction coefficient, is significantly improved when the model D is introduced.

10. Conclusions

In this work, we studied a method for correcting the Reynolds stress tensor using Pope's approach and DNS data. This new method comprises two stages: (i) data assimilation is used to identify a non-linear correction to the Boussinesq assumption, (ii) a neural network is trained to correct the characteristic time using RANS simulations to minimize the prediction error. The RANS model including the neural network augmented turbulence model and the non-linear Reynolds stress correction is then used to perform out-of-sample simulations. The presented method underwent validation on multiple geometries of a periodic hill configuration while maintaining a constant Reynolds number, in addition to being applied to the NASA hump test case. These flow configurations show significant separation phenomena, making them ideal benchmarks for assessing the predictive capabilities of the newly developed model for fully developed turbulent flows. The results obtained from out-of-sample configurations demonstrate a notable enhancement in the velocity profiles of RANS simulations, achieved through the implementation of the new correction in comparison to the standard SST model. A crucial aspect of our study focused on the integration of realizability conditions during the training process of the data-augmented model. Through rigorous testing, we found that overlooking this aspect during training could result in significant violations of the realizability conditions during the prediction phase. To address this issue, we introduced realizability constraints by means of penalization in both steps (i) and (ii) of the proposed procedure. By carefully considering the realizability

conditions and incorporating the penalization method, our approach ensures the validity and accuracy of the predictions, leading to more reliable and consistent outcomes in RANS simulations. Despite these encouraging results, data driven turbulence modeling comes with challenges, particularly concerning numerical stability issues. The complex interplay between the Reynolds stress corrections and the numerical integration scheme requires careful consideration to ensure that the coupling is stable and that the simulation results remain physically meaningful. The use of RANS simulations in the optimization loop to identify the correct characteristic time mitigate these difficulties. However, our future efforts will be dedicated to exploring techniques to address these stability challenges, with the ultimate goal of achieving more reliable and accurate predictions in turbulent flow simulations for a wide range of applications.

Acknowledgments

The authors acknowledge funding from Italian Ministry of University and Research: PRIN research project 2022B2X937, "NextGenSProDesT Next Generation Space Propulsion Design Techniques".

References

Balay, S., Gropp, W.D., McInnes, L.C. and Smith, B.F. (1997), *Efficient Management of Parallelism in Object Oriented Numerical Software Librarie*s, Modern Software Tools in Scientific Computing, Birkhauser Press.

Barth, T.J. and Jespersen, D.C. (1989), "The design and application of upwind schemes on unstructured meshes", *AIAA 27th Aerospace Sciences Meeting*, Reno, January. https://doi.org/10.2514/6.1989-366.

Broyden, C.G. (1969), "A new double-rank minimization algorithm", *Notic. Am. Math. Soc.*, **16**, 670.

Ferrero, A. and D'Ambrosio, D. (2020), "A hybrid numerical flux for supersonic flows with application to rocket nozzles", *Adv. Aircraft Spacecraft Sci.*, **7**(5), 387-404. https://doi.org/10.1063/5.0026763.

Ferrero, A., Iollo, A. and Larocca, F. (2019), "RANS closure approximation by artificial neural networks", *ETC 2019-13th European Turbomachinery Conference on Turbomachinery Fluid Dynamics and Thermodynamics*, Lausanne, Switzerland, April.

Ferrero, A., Iollo, A. and Larocca, F. (2020), "Field inversion for data-augmented RANS modelling in turbomachinery flows", *Comput. Fluid.*, **201**, 104474. https://doi.org/10.1016/j.compfluid.2020.104474.

Foures, D.P.G., Dovetta, N., Sipp, D. and Schmid, P.J. (2014), "A data-assimilation method for Reynolds-averaged Navier-Stokes-driven mean flow reconstruction", *J. Fluid Mech.*, **759**, 404-431. https://doi.org/10.1017/jfm.2014.566.

Geuzaine, G. and Remacle, J.F. (2009), "Gmsh: a three-dimensional finite element mesh generator with built-in pre- and post-processing facilities", *Int. J. Numer. Meth. Eng.*, **79**(11), 1309-1331. https://doi.org/10.1002/nme.2579 .

Greenblatt, D., Paschal, K.B., Yao, C.S., Harris, J., Schaeffler, N.W. and Washburn, A.E. (2006), "Experimental investigation of separation control Part 1: Baseline and Steady Suction", *AIAA J.*, **44**(12), 2820-2830. https://doi.org/10.2514/1.13817.

Holland, J.H. (1992), "Genetic algorithms", *Scientif. Am.*, **267**(1), 66-73.

Ling, J. and Templeton, J. (2015), "Evaluation of machine learning algorithms for prediction of regions of high Reynolds averaged Navier Stokes uncertainty", *Phys. Fluid.*, **27**, 085103. https://doi.org/10.1063/1.4927765.

Ling, J., Kurzawski, A. and Templeton, J. (2016), "Reynolds averaged turbulence modelling using deep neural networks with embedded invariance", *J. Fluid Mech.*, **807**, 155-166.

https://doi.org/10.1017/jfm.2016.615.
Menter, F.R. (1994), "Two-equation eddy-viscosity turbulence models for engineering applications", *AIAA J.*, **32**(8), 1598-1605. https://doi.org/10.2514/3.12149.
Nelder, J.A. and Mead, R. (1965), "A simplex method for function minimization", *Comput. J.*, **7**, 308-313. https://doi.org/10.1093/comjnl/7.4.308.
Pandolfi, M. (1984), "A contribution to the numerical prediction of unsteady flows", *AIAA J.*, **22**(5), 602-610. https://doi.org/10.2514/3.48491.
Parish, J.L. and Duraisamy, K. (2016), "A paradigm for data-driven predictive modeling using field inversion and machine learning", *J. Comput. Phys.*, **305**, 758-774. https://doi.org/10.1016/j.jcp.2015.11.012.
Parneix, S., Laurence, D. and Durbin, P.A. (1998), "A procedure for using DNS databases", *J. Fluid. Eng.*, **120**(1), 40-47. https://doi.org/10.1115/1.2819658.
PETSc (2023), Portable, Extensible Toolkit for Scientific Computation. https://petsc.org/
PETSc/TAO Users Manual (2023), Technical Report ANL-21/39-Revision 3.19, Argonne National Laboratory.
Pope, S. (1975), "A more general effective-viscosity hypothesis", *J. Fluid Mech.*, **72**(2), 331-340. https://doi.org/10.1017/S0022112075003382.
Powell, M.J.D. (1964), "An efficient method for finding the minimum of a function of several variables without calculating derivatives", *Comput. J.*, **7**, 155-162. https://doi.org/10.1093/comjnl/7.2.155.
Rumsey, C., Smith, B. and Huang, G. (2010), "Description of a website resource for turbulence modeling verification and validation", *AIAA 40th Fluid Dynamics Conference and Exhibit*, Chichago, USA, June-July. https://doi.org/10.2514/6.2010-4742.
Rusanov, V.V. (1962), "The calculation of the interaction of nonstationary shock waves and obstacles", *USSR Comput. Math. Math. Phys.*, **1**(2), 304-320. https://doi.org/10.1016/0041-5553(62)90062-9.
Sandberg, R.D. and Michelassi, V. (2019), "The current state of high-fidelity simulations for main gas path turbomachinery components and their industrial impact", *Flow Turbul. Combus.*, **102**, 797-848. https://doi.org/10.1007/s10494-019-00013-3.
Sandberg, R.D. and Weatheritt, J. (2014), "A novel evolutionary algorithm applied to algebraic modifications of the RANS stress-strain relationship", *J. Comput. Phys.*, **325**, 73-94. https://doi.org/10.1016/j.jcp.2016.08.015.
Singh, A.P., Medida, S. and Duraisamy, K. (2017), "Machine-learning-augmented predictive modeling of turbulent separated flows over airfoils", *AIAA J.*, **55**(7), 2215-2227. https://doi.org/10.2514/1.J055595.
Wang, J.X., Wu, J.L. and Xiao, H. (2017), "Physics-informed machine learning approach for reconstructing Reynolds stress modeling discrepancies based on DNS data", *Phys. Rev. Fluid.*, **2**, 034603. https://doi.org/10.1103/PhysRevFluids.2.034603.
Wu, J.L., Wang, J.X., Xiao, H. and Ling, J. (2017), "A priori assessment of prediction confidence for data driven turbulence modeling", *Flow Turbul. Combus.*, **99**, 25-46. https://doi.org/10.1007/s10494-017-9807-0.
Wu, J.L., Xiao, H. and Paterson, E. (2018), "Physics-informed machine learning approach for augmenting turbulence models: A comprehensive framework", *Phys. Rev. Fluid.*, **3**(7), 074602. https://doi.org/10.1103/PhysRevFluids.3.074602.
Xiao, H. and Cinnella, P. (2019), "Quantification of model uncertainty in RANS simulations: A review", *Progr. Aerosp. Sci.*, **108**, 1-31. https://doi.org/10.1016/j.paerosci.2018.10.001.
Xiao, H., Wu, J.L., Laizet, S. and Duan, L. (2020), "Flows over periodic hills of parameterized geometries: A dataset for data-driven turbulence modeling from direct simulations", *Comput. Fluid.*, **200**, 104431. https://doi.org/10.1016/j.compfluid.2020.104431.
Zhao, Y., Akolekar, H.D., Weatheritt, J., Michelassi, V. and Sandberg, R.D. (2020), "RANS turbulence model development using CFD driven machine learning", *J. Comput. Phys.*, **411**, 109413. https://doi.org/10.1016/j.jcp.2020.109413.